JOURNAL OF AIRCRAFT
Vol. 30, No. 3, May–June 1993

Computational Investigation of a Pneumatic Forebody Flow Control Concept

Ken Gee*
MCAT Institute, Moffett Field, California 94035
Domingo Tavella†
Stanford University, Stanford, California 94305
and
Lewis B. Schiff‡
NASA Ames Research Center, Moffett Field, California 94035

The effectiveness of a tangential slot blowing concept for generating lateral control forces on an aircraft forebody is analyzed using computational fluid dynamics (CFD). The flow about a fighter forebody is computed using a multiple-zone, thin-layer Navier-Stokes code. Tangential slot blowing is modeled by the use of an actuator plane. The effects of slot location and slot length on the efficiency of the system are analyzed. Results of the study indicates that placement of the slot near the nose of the aircraft greatly enhances the efficiency of the system, whereas, the length and circumferential location of the slot are of secondary importance. Efficiency is defined by the amount of side force or yawing moment obtained per unit blowing coefficient. The effect of sideslip on the system is also analyzed. The system is able to generate incremental changes in forces and moments in flow with a sideslip angle of 10 deg comparable to those obtained at zero sideslip. These results are used to determine a baseline configuration for an experimental study of the tangential slot blowing concept.

Nomenclature

A_j = area of the slot
A_{ref} = reference area, wing area, 400 ft^2
C_n = yawing moment coefficient, $n/q_\infty A_{ref}\bar{c}$
$C\mu$ = blowing coefficient, $\rho_j A_j V_j^2/q_\infty A_{ref}$
C_Y = side force coefficient, $Y/q_\infty A_{ref}$
$\bar{c}$ = wing mean aerodynamic chord, 11.52 ft
c_y = local side force coefficient, $y/q_\infty A_{ref}$
h_s = height of the slot
l = axial length along the body
M_j = jet exit Mach number
M_∞ = freestream Mach number
P_j = jet static exit pressure
P_0 = jet total pressure
q_∞ = freestream dynamic pressure
$Re_{\bar{c}}$ = Reynolds number based on freestream conditions and mean aerodynamic chord
T_j = jet static exit temperature
u_m = maximum local velocity
V_j = jet exit velocity
x, y, z = physical coordinates
α = angle of attack
β = sideslip angle
ζ = normal distance from the surface
ζ_m = distance from surface to maximum local velocity
η_b = efficiency of slot blowing system, C_y/C_μ
μ_t = turbulent eddy viscosity coefficient
ξ, η, ζ = computational coordinates in axial, circumferential, and normal directions
ρ = local density
ρ_j = jet exit density
ρ_∞ = freestream density
ϕ = slot location circumferential angle, measured from windward plane of symmetry

Presented as Paper 91-3249 at the AIAA 9th Applied Aerodynamics Conference, Baltimore, MD, Sept. 23–25, 1991; received Dec. 7, 1991; revision received March 12, 1992; accepted for publication March 13, 1992.

*Research Scientist, MS 258-1. Member AIAA.
†Research Associate; currently at CSC Corporation, Ames Research Center, Moffett Field, CA. Member AIAA.
‡Special Assistant for High Alpha Technology, Fluid Dynamics Division, MS 258-1. Associate Fellow AIAA.

Introduction

A TOPIC of current research is the control of high-performance aircraft at high angles of attack. The ability of a pilot to maneuver his aircraft while flying at high incidence enhances agility and improves the safety of the aircraft. However, the controllability of current fighter aircraft dramatically decreases as the angle of attack increases. In general, controllability of an aircraft such as the NASA F/A-18 high alpha research vehicle (HARV) is reduced at high incidence because the vertical tails are immersed in the wake region of the wing. In order to maintiain directional controllability at this attitude, addtitional yawing moment is needed.

Various methods of providing additional yaw control power are being investigated. Within NASA, the high alpha technology program is currently in the process of testing several methods to enhance control of an aircraft at high incidence. These methods include the use of thrust vectoring (e.g., Ref. 1), movable forebody strakes (e.g., Ref. 2), and pneumatic forebody flow control (e.g., Ref. 3). In this study, a pneumatic forebody flow control concept is studied using computational fluid dynamics (CFD) to determine if the concept can provide the desired control forces and moments in high Reynolds number flows. The pneumatic control "system" is composed of a slot on the aircraft forebody through which air is ejected into the boundary layer tangential to the body surface. The wall jet created by the blowing remains attached to the surface up to a new separation line. The interaction of the new flow structures due to blowing with the rest of the flowfield creates yawing forces and moments that are useful in controlling the aircraft.

The tangential slot blowing concept has been tested in water tunnels at laminar Reynolds numbers with encouraging results[4] and in wind tunnels on subscale models.[3] Previous compu-

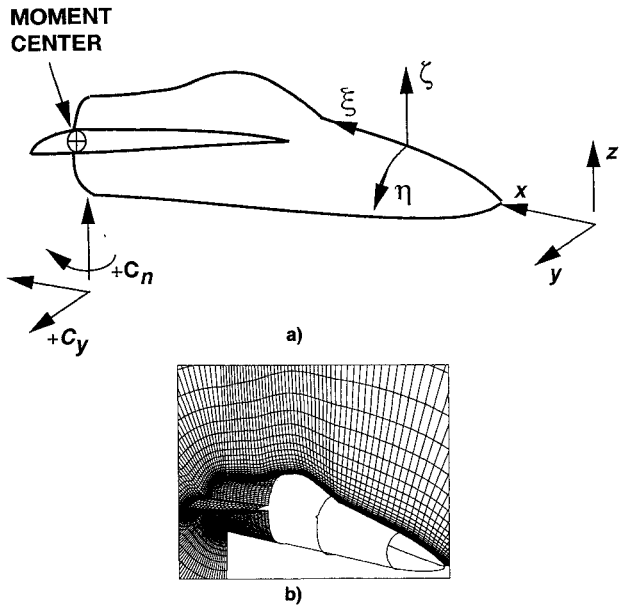

Fig. 1 Schematic of body and grid used in computations: a) coordinate systems, grid boundaries, and moment center; and b) portion of grid and grid boundaries.

tational studies on a body of revolution[5,6] and a fighter forebody[7,8] show that such a system can provide control power at high angle of attack approximating that obtained from vertical tails at low angle of attack. Present research on this concept is aimed at finding an effective slot length and slot location on the HARV, and to determine the effects of sideslip on the system. The results of this study, in addition to previous subscale experimental data, are used to develop a baseline model for a system to be tested in a full-scale wind-tunnel experiment.

In the current work, a multizone, thin-layer Navier-Stokes code is used to compute the flow about the HARV forebody, which includes the nose and leading-edge extension (LEX) up to the leading edge of the wing (Fig. 1a). The flow solver, grid, turbulence models, and boundary conditions are briefly described in the next section. The following section describes the slot geometries investigated. In this study, only the slot location and length are varied. Finally, the computational results obtained from this study are analyzed.

Numerical Method

The equations governing fluid motion are combined to form the Navier-Stokes equations, a set of five coupled, nonlinear partial differential equations. The full equations define fluid motion in complete detail. Simplified forms of the Navier-Stokes equations are generally used in computational work. For a body-oriented coordinate system (ξ, η, ζ), in which one of the coordinates is approximately normal to the body surface (Fig. 1a), the thin-layer approximation is used, in which only the viscous terms in the body-normal, or ζ, direction are retained. The thin-layer Navier-Stokes equations, written in terms of nondimensional variables,[9] can be expressed as

$$\partial_\tau \hat{Q} + \partial_\xi \hat{F} + \partial_\eta \hat{G} + \partial_\zeta \hat{H} = Re^{-1}\partial_\zeta \hat{S} \qquad (1)$$

In Eq. (1) the viscous terms are collected into the vector S and the nondimensional Reynolds number Re is factored from the viscous flux term.

Numerical Algorithm

The numerical scheme used in this study is the implicit F3D code reported by Steger et al.[10] The algorithm uses flux-vector splitting[11] to upwind difference the convection terms in the nominally streamwise coordinate direction, while central differencing is used in the other two directions. This code has been used to compute the flowfield about bodies of revolution at high incidence (e.g., Refs. 12 and 13), complex aircraft geometries such as the isolated F-18 HARV fuselage (e.g., Ref. 14), and the complete F-18 configuration (e.g., Refs. 15 and 16) at high angle-of-attack flight conditions. The results of these studies show that the code can accurately predict the complex character of three-dimensional separated flow. Thus, the code is well-suited for use in this study. Full details of the algorithm and its development are found in Refs. 10 and 17.

Turbulence Models

Closure of the governing equations is achieved by using a turbulence model to obtain the eddy viscosity values. In this study, the Baldwin-Lomax algebraic turbulence model[18] with the Degani-Schiff modifications[19] is used in all regions except the jet, where a model based on work by Roberts[20] for turbulent curved wall jets is applied.

The Baldwin-Lomax model with the Degani-Schiff modifications has been used extensively in three-dimensional high-incidence problems with good success. Previous computations of flow about the F-18 forebody[14] using this model closely predicted the separation line locations observed on the nose and wing leading-edge extension (LEX) of the aircraft in flight. The computed surface pressure distributions compared well with flight test data. Therefore, the use of this code and turbulence model is a proven choice for the current study.

In the slot region, a different turbulence model is used to account for the turbulent wall jet caused by the blowing. For this portion of the flow, a model based on work by Roberts[20] is used. This model has been used by Yeh et al.[21] to compute flows about thick, rounded leading-edge delta wings with tangential leading-edge slot blowing. It uses self-similar profiles for the mean velocity and momentum balance to obtain an expression for the eddy viscosity. Making use of experimental data, an equation is derived for the eddy viscosity

$$\mu_t = 0.0033\zeta_m \rho u_m (\bar{\zeta}/\bar{\zeta}_m)^2 \qquad (2)$$

where $\bar{\zeta}$ is the normal distance from the wall, and the subscript m denotes the values at the maximum velocity location. This model is applied in the region between the slot and the point where the velocity vector in the circumferential direction reverses sign.

Grids and Boundary Conditions

The grid used in the computations defines the nose and LEX of the F-18 (Fig. 1b), with the tip of the nose located at $x = 5.1$ ft in cartesian space, and the back plane of the grid located at $x = 34.25$ ft. The dimensions are equivalent to that on the aircraft. The nose begins at $x = 5.1$ ft to be consistent with the aircraft blueprints. The grid has a total of 518,000 grid points. In the section extending from the nose to the beginning of the LEX, there are 35 axial points, 101 circumferential points that describe the complete forebody, and 50 radial points from the surface to the outer boundary, which is located approximately eight body diameters away from the surface. The section that contains the LEX has 36 axial points, 165 circumferential points, and 50 radial points. This grid resolution was previously used in Ref. 14 for isolated F-18 forebody computations, and shown to give adequate definition of the main flow structures. The present grid is divided into 12 zones, with point-to-point matching between zones. The number of zones is dictated in part by the computer memory requirements and in part by the modeling requirements of the slot. Boundary conditions are passed between zones by direct injection where there is a zonal overlap, and interpolation where no overlap exists. The orientation of cartesian and computational space coordinates are shown in Fig. 1a.

Freestream conditions are maintained at the inflow and outer boundaries. A zero-axial-gradient extrapolation is used at the outflow plane. A no-slip condition is applied at the

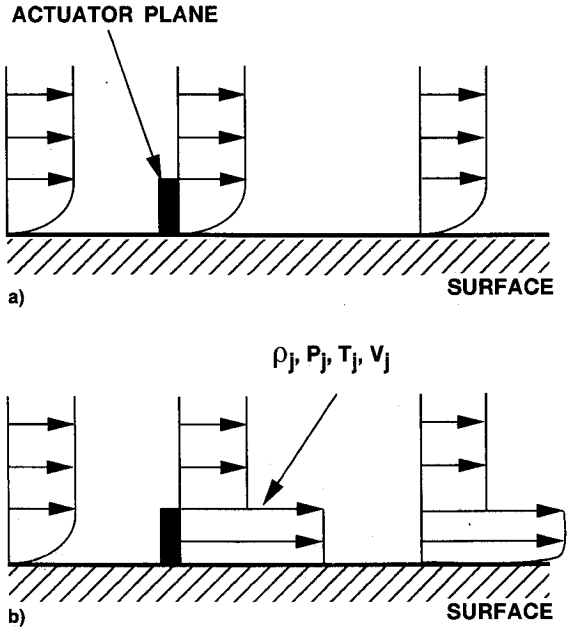

Fig. 2 Schematic showing actuator plane concept: a) no blowing, and b) blowing.

body surface. These are identical to the conditions used in the F-18 forebody computations.[14] However, unlike Ref. 14, the grid extends completely around the body circumferentially since the flowfield will be asymmetric due to the blowing or the presence of sideslip.

To model the slot, an actuator plane is used (Fig. 2). The grids are defined such that the slot lies along the boundary between two grid zones (Fig. 1b). The actuator plane is part of the windward boundary of the upper grid (Fig. 1b). There is no overlap between the two zones. The boundary values for the lower grid are obtained by zeroth-order extrapolation using the interior points of the grid for both the no-blowing and blowing case. For the no-blowing case, no new boundary conditions are introduced at the actuator plane, and the flow variables at the upper grid boundary are obtained by interpolation using the values at the grid points on either side (Fig. 2a).

For the blowing case, the flow variables in the actuator plane are overwritten with the jet conditions (Fig. 2b). It is assumed that P_0 is known and is equal to 1.415 times the ambient pressure P_∞. The total pressure is used to determine M_j by assuming that the exit pressure P_j is equal to freestream, and the flow is isentropic. For the chosen pressure ratio, $M_j = 0.72$. Upon setting T_j to the freestream value, the density and energy of the jet are determined. Note that setting the jet exit pressure to freestream introduces a slight error into the computations since the local pressure at the jet exit is not precisely that of the freestream, but this error is slight and the flow recovers quickly from the discontinuity. These slot boundary conditions are identical to those used in the previous computations by Tavella et al.[7] All the slot geometries investigated in this study have the same P_0 and M_j. As a result, the jet mass flux and momentum coefficients are dependent only upon the area of the slot.

Results and Discussion

The flow about the forebody of the F-18 is computed using the flow solver described in the previous section. The grid used in these computations is shown in Fig. 1b. To accommodate the actuator plane, the grid is divided into zones such that the slot lies along the boundary between two zones. Due to computer memory limitations, the grid is further divided into a total of 12 zones. Steady-state solutions are obtained using a Cray Y-MP or a Cray-2 supercomputer. Typical solutions required 4MW of memory and about 40 Cray-2 CPU hours for convergence.

The flow conditions in all cases are $M_\infty = 0.20$, $\alpha = 30$ deg, and $Re_{\bar{c}} = 11.52 \times 10^6$. Cases are obtained for flow with no sideslip, $\beta = 0$ deg, and with a sideslip angle of $\beta = -10$ deg, to determine how sideslip influences the control forces generated by the slot blowing system. Several slot geometries are investigated at zero sideslip to determine the effects of slot location and slot length on the effectiveness of the control system. The efficiency of the system η_b is measured by the amount of side force and yawing moment that is obtained per unit momentum blowing coefficient. The momentum blowing coefficient C_μ is defined as

$$C_\mu = (\rho_j A_j V_j^2 / q_\infty A_{\text{ref}}) = (\dot{m}_j V_j / q_\infty A_{\text{ref}}) \tag{3}$$

Slot Configurations

The slot configurations investigated differ in the length of the slot and the location of the slot on the forebody. All of the slots used in this study have a nominal height h_j of 0.013 ft, and all slots have the same pressure ratio, P_0/P_j, and jet exit Mach number M_j. The initial slot configuration studied is 5.7-ft long, with its leading edge located 4.6 ft from the nose (Fig. 3a). The slot is set at a circumferential angle of $\phi = 112$ deg, measured from the windward plane of symmetry. The blowing coefficient for this slot is $C_\mu = 0.005$. A similar slot configuration was used in subscale experimental work by Schreiner.[3] Computed solutions obtained for this configuration were originally reported in Ref. 7.

It is well recognized, from both experimental and computational studies, that small disturbances placed close to the nose of a body of revolution at large incidence produce large asymmetries in the flow (e.g., Refs. 22 and 23). Using this principle as a guide, a second slot design was developed. This configuration has a 3.6-ft-long slot located only 0.4 ft from the nose (Fig. 3b). For this slot geometry, $C_\mu = 0.0027$. The length of the slot is dictated in part by the desire to place the entire length of the slot within the radome of the test aircraft. Two circumferential locations are studied, with $\phi = 112$ deg and $\phi = 90$ deg.

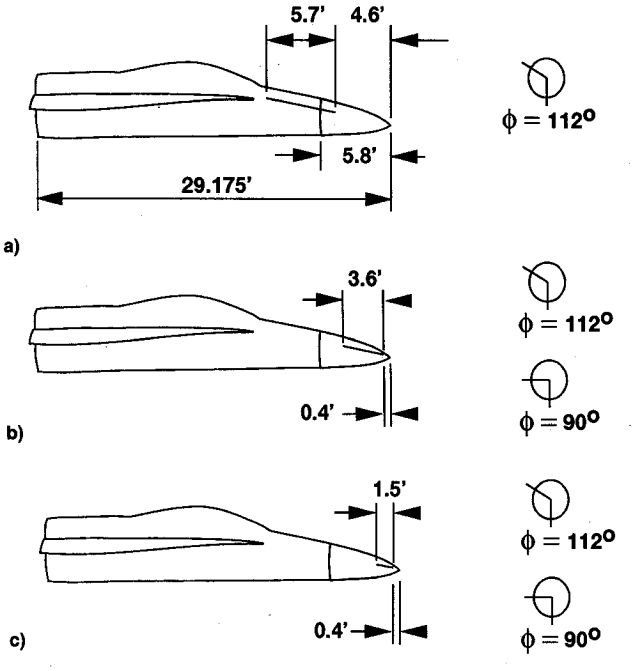

Fig. 3 Slot configurations: a) 5.7-ft slot, b) 3.6-ft slot, and c) 1.5-ft slot.

The final slot configuration is a shortened version of the previous slot. The length of the slot is reduced from 3.6 to 1.5 ft, while the leading edge of the slot remains located 0.4 ft from the nose of the aircraft (Fig. 3c). For this slot, $C\mu$ = 0.0013. Again, two circumferential locations are studied, with ϕ = 112 deg and ϕ = 90 deg. Shortening the slot has the benefit of reducing the blowing coefficient of the configuration. However, it has been found for bodies of revolution at high incidence that varying the size of the perturbation at a fixed location on the body has a large effect on the side force obtained.[23,24] Thus, it is necessary for the present configuration to determine how shortening the slot will affect the character of the flowfield and the efficiency of the system.

Forces and Moments at Zero Sideslip

One of the thrusts of this study is to determine an efficient slot configuration to be used for further study in wind-tunnel experiments. Efficiency is defined as the amount of side force and yawing moment obtained per unit momentum blowing coefficient. Forces and moments are obtained by integrating the surface pressure distribution only. Positive side force is defined such that it moves the body in the positive direction of the y axis. Positive yawing moment turns the nose of the body in a clockwise direction (Fig. 1).

For the case of zero sideslip, the computed side-force coefficient for each configuration is plotted as a function of its momentum coefficient in Fig. 4. As the length of the slot is reduced, C_μ is reduced, but the amount of side force does not drop significantly. Even though the 5.7-ft slot generates the largest incremental change in C_Y, it is the least efficient of the slot configurations studied, with η_b = 13.0. The 1.5-ft slot proves to be the most efficient, with η_b = 38.5. This is due to the shorter slots being located closer to the nose of the aircraft. A large gain in efficiency is obtained by using the 1.5-ft slot, since there is only a small loss in side force for a reduction of C_μ by a factor of two, when compared with the 3.6-ft slot. From these results, a short slot near the nose of the aircraft provides the most lateral control force for the smallest amount of C_μ.

For the two short slots, locating the slot further towards the windward side (ϕ = 90 deg) reduces the side force by about 6%, in comparison with the same length slot located at ϕ = 112 deg (Fig. 4). Analogous trends may be seen for the computed yawing-moment coefficient (Fig. 5). Note that the moments are taken about the back plane of the computational grid, which is 29.175 ft from the nose of the aircraft (Fig. 3), or 34.25 ft from the origin of the physical coordinate frame.

Flow Characteristics at Zero Sideslip

One method of understanding the changes in the flowfield due to the slot blowing is by studying the surface flow patterns. The surface flow pattern is obtained by integrating the velocity vectors located one grid point above the surface.

The surface flow pattern obtained from the no-blowing solution (Fig. 6a) shows good agreement with surface flow patterns obtained from flight experiments.[14] The primary and secondary crossflow separation lines on the forebody are clearly seen, as well as the secondary separation lines on the LEX.

Comparing the baseline flow pattern with that obtained from the solution using the 3.6 ft slot (Fig. 6b) shows the effect of slot blowing on the flowfield. In the slot region, the jet remains attached to the surface well past the leeward plane of symmetry so that only one primary separation line appears, located on the nonblowing side. At this line, the jet separates from the surface. Aft of the slot, on the blowing side, a separation line forms at about the same circumferential location as the primary separation line of the no-blowing case. Shortening the slot from 3.6 to 1.5 ft changes the surface flow pattern slightly (Fig. 6c). The jet separation line on the nonblowing side is located further towards the leeward plane of symmetry. The crossflow separation line that forms aft of the

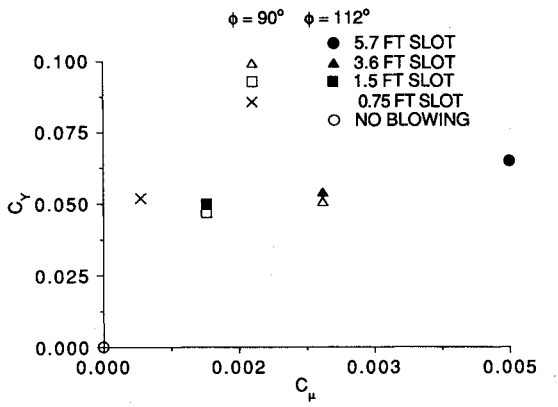

Fig. 4 Effect of slot length and location on side-force coefficient; M_∞ = 0.20, α = 30 deg; Re_c = 11.52 × 10⁶.

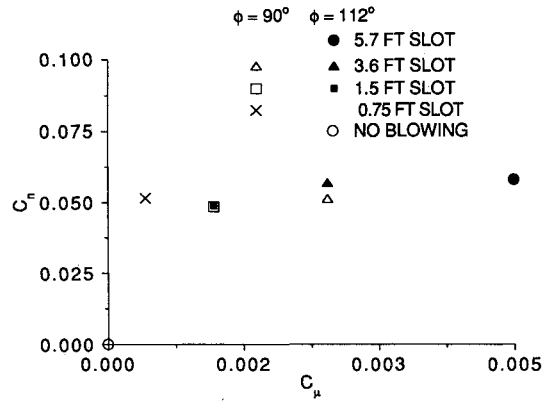

Fig. 5 Effect of slot length and location on yawing-moment coefficient; M_∞ = 0.20, α = 30 deg, Re_c = 11.52 × 10⁶.

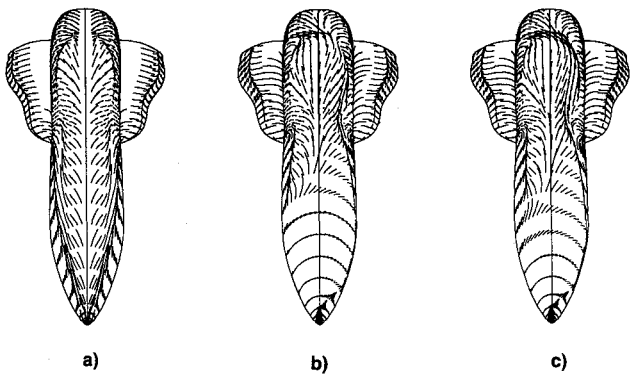

Fig. 6 Surface flow patterns for solutions with no sideslip; M_∞ = 0.20, α = 30 deg, Re_c = 11.52 × 10⁶: a) no blowing; b) 3.6-ft slot, right side, ϕ = 112 deg; and c) 1.5-ft slot, right side, ϕ = 112 deg.

slot on the blowing side is located further leeward as well. Since the slot is shorter, the flow begins to turn downstream much sooner in the 1.5-ft slot solution (Fig. 6c) than in the 3.6-ft slot solution (Fig. 6b). The flow patterns in the aft portion of the body show some slight changes. The LEX secondary separation lines move slightly inboard in the solutions with blowing (Figs. 6b and 6c). The flow is also asymmetric in the region of the canopy. These changes in the flowfield between the 3.6- and 1.5-ft slot solutions account in part for the differences in the side force and yawing moment obtained for these two blowing cases.

Helicity density contours[25] help visualize the changes in the off-body flowfield due to blowing (Fig. 7). In this figure the lines represent constant values of helicity density with the largest values located in the core of the vortices. Solid lines represent clockwise rotation of the flow, while dashed lines represent counterclockwise rotation, when viewed from the front of the aircraft. There are observable differences in the

relative strength of the LEX primary vortices between the no-blowing (Fig. 6a) and blowing solutions (Figs. 6b and 6c). Overall, the no-blowing solution has a stronger set of LEX primary vortices than do the blowing solutions. However, the primary LEX vortices are initially stronger in the blowing cases, causing the secondary vortices to be stronger as well. This may be due to the different numerical smoothing values used in the nonblowing and blowing solutions. The second-order smoothing coefficient was set at 0.015 in the nonblowing case, whereas it was set at 0.030 in the blowing cases to help damp out oscillations in the far field. However, it is expected that this numerical difference is small compared to the physical changes due to the existence of the jet in the flow. The LEX primary vortex on the nonblowing side is weaker than the one on the blowing side in Figs. 6b and 6c. The interaction between the forebody vortex structure due to the jet and the flowfield over the LEX causes the asymmetry seen in the blowing solutions. Furthermore, the helicity contours indicate a vortical structure close to the surface in the area of the canopy for the slot blowing cases (Figs. 7b and 7c) which does not exist in the no-blowing case (Fig. 7a). This asymmetry near the canopy causes the surface pressure on the blowing side to be lower than the pressure on the nonblowing side.

A change in the circumferential location of the slot from $\phi = 112$ to $\phi = 90$ deg alters the forebody vortical structures and the structure over the canopy (Fig. 8). For the 1.5 ft slots, the primary forebody vortex creates regions of vorticity that separates from the body along the axial direction. However, for the slot at $\phi = 90$ deg, there is a region of clockwise helicity on the nonblowing side of the canopy area (Fig. 8b) which is not apparent in the solution with the slot at $\phi = 112$ deg (Fig. 7c). The LEX vortices do not exhibit any noticeable differences between the two solutions. The differences near the nose and over the canopy and LEX region accounts for the difference in side force and yawing moment between these two cases.

The change in the local surface pressure in the LEX region helps explain how tangential slot blowing generates side force. In the slot region, a low pressure region is caused by the jet remaining attached to the surface, whereas on the nonblowing side, the flow has separated and a higher pressure region exists. Changes in the flowfield near the nose due to blowing cause changes in surface pressure, and thus the local side-force distribution, along the entire body (Fig. 9a). For cases with zero sideslip, there is a positive side force (force acting in the $\pm y$ direction) along the entire length of the body. The side force is due mainly to the interaction of the new flowfield caused by the jet on the nose with the remainder of the flowfield. Note that a circumferential change in the slot location from $\phi = 112$ to $\phi = 90$ deg (Fig. 9b) for the 1.5-ft slot increases the side force in the slot region. However, the side force along the remainder of the body is reduced. Thus, the slot located at $\phi = 90$ deg generates slightly less total side force than the slot located at $\phi = 112$ deg. Results computed using the 3.6-ft slot are similar.[8] It appears that the mechanism in slot blowing which generates the side force and yawing moment is the interaction of the separated jet vortical structure with the remainder of the flowfield. Exactly how this mechanism works remains a subject of further study.

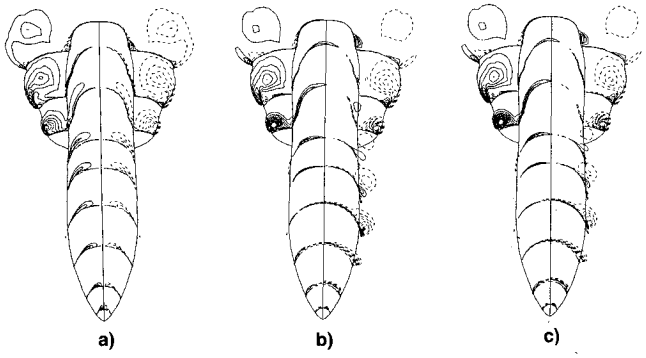

Fig. 7 Helicity density contours for solutions with no sideslip; M_∞ = 0.20, α = 30 deg, Re_c = 11.52 × 10^6: a) no blowing; b) 3.6-ft slot, right side, ϕ = 112 deg; and c) 1.5-ft slot, right side, ϕ = 112 deg.

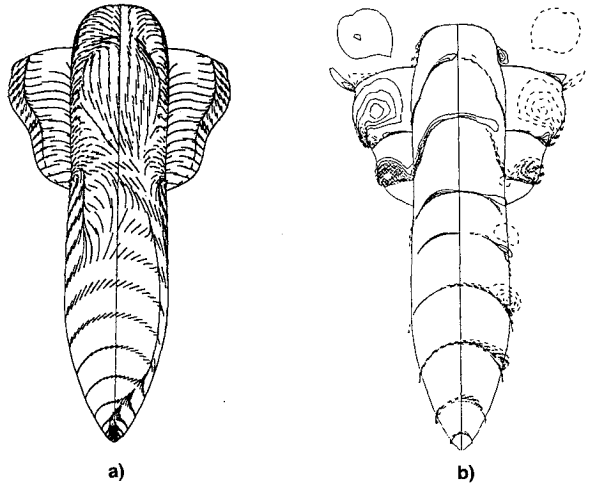

Fig. 8 Visualization of solution with 1.5-ft slot at ϕ = 90 deg, M_∞ = 0.20, α = 30 deg, Re_c = 11.52 × 10^6: a) surface flow pattern, and b) helicity density contours.

Flow Characteristics with Sideslip

The effects of sideslip were studied by obtaining solutions using the 3.6-ft slot located at $\phi = 112$ deg and a sideslip of $\beta = -10$ deg (Fig. 10), with all other parameters the same as in the no-sideslip case. Blowing from slots on the pilot-right and pilot-left side of the fuselage are investigated. Since the forebody blowing concept apparently generates lateral control by keeping the jet attached to the surface and displacing the forebody vortices, the effectiveness of the concept may be degraded when the aircraft is flying at an angle of sideslip. In this case, the separation lines and vortices are displaced from symmetry due to the oncoming wind. This

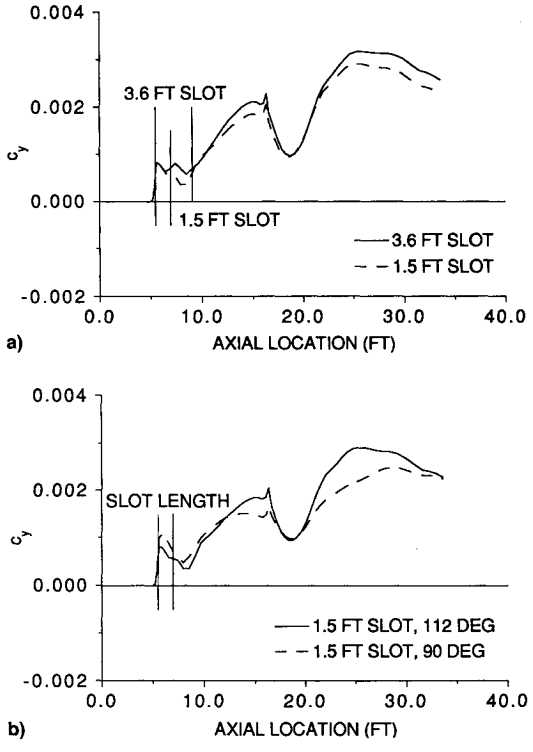

Fig. 9 Side-force distribution along the body; M_∞ = 0.20, α = 30 deg; Re_c = 11.52 × 10^6: a) effect of slot length at ϕ = 112 deg, and b) effect of slot circumferential location for 1.5-ft slot.

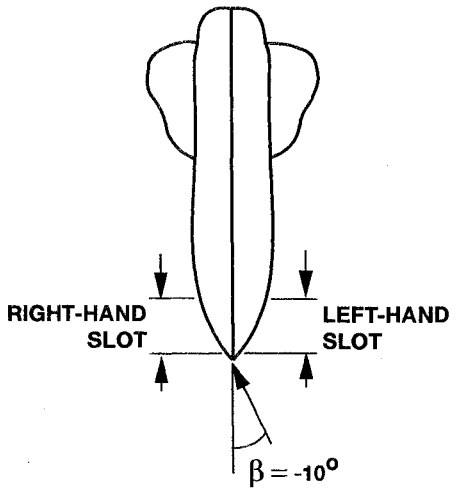

Fig. 10 Schematic of sideslip direction and slot orientation for cases with sideslip.

behavior is clearly shown in the no-blowing surface flow pattern with $\beta = -10$ deg (Fig. 11a). On the forebody, the windward primary separation line is rotated almost to the leeward centerline, with the separation line extending over the canopy. The leeward separation line rotates in similar fashion away from the wind direction. The LEX secondary crossflow separation line is also affected by the wind direction. The windward LEX primary vortex and secondary crossflow separation line are moved inboard, while the primary vortex and secondary crossflow separation line on the leeward LEX is shifted outboard.

For the blowing system to be effective, it must generate enough side force and yawing moment to overcome the force and moment imparted on the entire aircraft due to the sideslip. However, the current study cannot predict such behavior since only the forebody is included in the computations. The contribution of the wings and empennage to the control of the aircraft, and the interaction of the new forebody flowfield due to blowing with these surfaces cannot be determined from this study, and will require further computational and experimental data. However, the present study does provide a good indication of the interaction of the forebody flow with the LEX flow in sideslip conditions.

The effect of blowing on the surface flow pattern for cases with sideslip is shown in Fig. 11. Blowing from a slot on the pilot right (Fig. 11b) produces a surface flow pattern similar to the no-sideslip case (Fig. 7b). In this case, the jet is moving in a direction opposite that of the local sideslip. The jet separation line is pushed well past the plane of symmetry, and although not shown in the figure, a separation line forms aft of the slot on the blowing side. No large changes are evident in the surface flow patterns on the LEX, but the flow in the canopy area is altered. The forebody primary separation line that extends over the canopy (Fig. 11a) no longer appears in the right blowing case (Fig. 11b).

Blowing from the opposite side of the fuselage (pilot's left) causes the blowing to augment the effect of the local sideslip. In this case, the jet is moving in the direction of the local sideslip. The blowing forces the jet separation line well past the symmetry plane (Fig. 11c), merging with the separation line on the nonblowing side. However, in this case a separation line forms aft of the slot in about the same location as the primary separation line in the nonblowing case (Fig. 11a). The jet separation line on the nonblowing side turns upward towards the leeward plane of symmetry, just as in the right blowing case. Similar to the case of blowing from the right side, no large changes are observed in the surface flow pattern on the LEX with blowing on the left.

Helicity density contours (Fig. 12) shows the changes in the forebody and LEX vortices due to the combined effect of sideslip and blowing. In the no blowing case (Fig. 12a), the

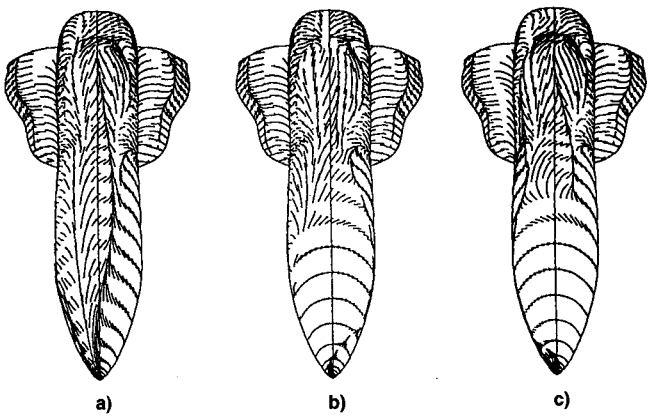

Fig. 11 Surface flow patterns for solutions with sideslip; $\beta = -10$ deg, $M_\infty = 0.20$, $\alpha = 30$ deg, $Re_c = 11.52 \times 10^6$: a) no blowing; b) 3.6-ft slot, right side, $\phi = 112$ deg; and c) 3.6-ft slot, left side, $\phi = 112$ deg.

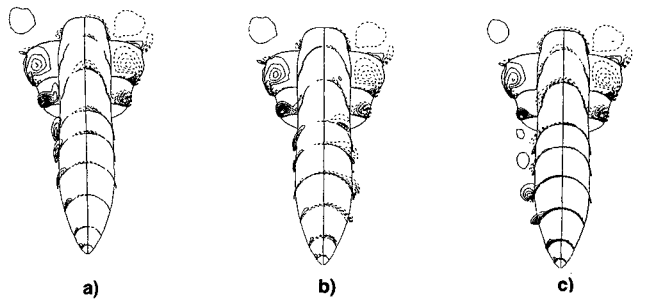

Fig. 12 Helicity density patterns for solutions with sideslip; $\beta = -10$ deg, $M_\infty = 0.20$, $\alpha = 30$ deg, $Re_c = 11.52 \times 10^6$: a) no blowing; b) 3.6-ft slot, right side, $\phi = 112$ deg; and c) 3.6-ft slot, left side, $\phi = 112$ deg.

two primary forebody vortices are clearly seen, with the windward vortex running along the centerline of the body over the canopy region. The windward LEX primary vortex is pushed closer to the body, while to leeward, LEX primary vortex is shown to be pushed outboard from the body.

Blowing from the right side alters the forebody flow structure in much the same way as blowing with no sideslip. However, there are changes in the LEX region. Blowing from the right side appears to weaken the windward primary LEX vortex, with no change observed in the leeward one. Weakening the windward LEX primary vortex causes an increase in the pressure on the windward side. Blowing from the left side has the opposite effect (Fig. 12c). In this case, the leeward LEX primary vortex is weakened and moved further outboard. This increases the pressure on the leeward side of the body. Also, the blowing has the direct effect of reducing the pressure on the nose such that a net force to the left is obtained. The net result of the changes in the pressure distribution is discussed in the next section.

Forces and Moments with Sideslip

As with the no-sideslip results, blowing in flows with sideslip generates forces and moments acting in the direction of the slot. That is, blowing from the right side causes positive increments in side force and yawing moment. Plotting the side-force coefficient against the sideslip angle shows this trend clearly (Fig. 13). For the case with zero sideslip, the no-blowing case still has zero side force, due to symmetry. Blowing on the right side produces a positive incremental change in the side-force coefficient. The side force is directed towards the side with the slot. Because of flow symmetry, the magnitude of the incremental change in side force due to blowing will be equal for blowing from the right and left side.

The same is not true for the cases with sideslip, since the no-blowing flow is no longer symmetrical. Blowing from the

right slot produces a positive incremental change in side force that is about 50% less than that obtained in the no-sideslip case. Blowing from the left side causes an incremental change in the negative direction that is about equal to that obtained for the no-sideslip case. Also, it can be seen that the change in side force obtained by blowing from the right side in a flow with negative sideslip is equivalent to that obtained by blowing from the left side in a flow with positive sideslip. Thus, the incremental changes in side force for cases with a positive sideslip angle of $\beta = +10$ deg shown in Fig. 13 are obtained from the solutions with a negative sideslip angle by reflection.

The trends observed in the side-force coefficient plot (Fig. 13) are also evident in a plot of the yawing-moment coefficient vs the sideslip angle (Fig. 14). At zero sideslip angle, flow symmetry dictates that the no-blowing case produces zero yawing moment. Blowing from the right side generates a positive incremental change in the yawing moment. With sideslip, the baseline no-blowing solution indicates the body undergoes a positive yawing moment. Blowing on the right side generates a positive incremental change in the moment (Fig. 14) that is slightly smaller than the change observed in the no-sideslip case. Blowing on the left side yields a negative incremental change that is about equal in magnitude with that for the no-sideslip case. The moment coefficients for the positive sideslip angle, $\beta = +10$ deg, are again obtained by reflecting the negative sideslip solutions. Data at smaller sideslip angles are required to determine the correct slope of the curves in Fig. 14, but certain trends can be obtained from the data points in hand.

Note that the side force due to the sideslip alone is negative (Fig. 15), whereas the yawing moment is positive (Fig. 14). This is due in part to the change in the LEX vortex structure. From Fig. 12, it was observed that the windward LEX primary vortex is displaced inboard, while the leeward LEX primary vortex is displaced outboard. Movement of the vortices causes a lower surface pressure on the windward side and a higher surface pressure on the leeward side, resulting in a side force in the negative direction. This negative force counteracts the positive side force due to the sideslip, causing a total side force in the negative direction.

This behavior can be clearly seen in the local side-force distribution along the body (Fig. 15). In the nose region, from 5.1 to 16.4 ft, the side force is positive, due to the sideslip. However, in the region of the LEX, the local side force increases, then drops and becomes negative as a result of the displacement of the vortices due to the sideslip. Integrating the side force distribution results in the side-force coefficient given in Fig. 13. Since the moment center is at the base of the body (Fig. 1), the region of positive side force has a larger moment arm than the region of negative side force, thus a positive yawing moment is obtained.

Blowing in cases with sideslip yields the following results. Blowing from the right side causes the side force distribution to be more positive along the entire body, whereas blowing from the left side causes the side force to be more negative along the entire body, when compared to the no-blowing case. These trends are almost opposite that found in the no-sideslip case (Fig. 9). In those solutions, the side force increases in the nose region, drops off near the beginning of the LEX, and increases again. For these cases, the entire side force distribution is positive. The reason for this behavior is due in part to the interaction of the jet separation vortex with the LEX vortex.

As noted previously, the LEX primary vortex on the nonblowing side is weaker than the one on the blowing side (Figs. 12b and 12c), causing the net side force in the LEX region to be towards the blowing side. However, near the beginning of the LEX the vortex due to the jet separation is still quite evident (Figs. 12b and 12c), creating a low pressure region and thus reducing the side force to the right. In the case with sideslip and blowing from the right side, the windward LEX primary vortex is weakened by the separated jet vortex (Fig. 12b) causing a more positive side force distribution. With blowing from the left, the leeward LEX primary vortex is weakened by the separated jet vortex (Fig. 12c) causing a more negative side force distribution. These observations indicate that the interaction of the vortex structures due to the blowing with the remainder of the flowfield is the primary reason for the incremental changes in the side force and yawing moment.

Further work must be done, both experimentally and computationally and using both simple and complex bodies, in order to fully understand the mechanisms that cause the large changes in the flowfield and the forces and moments due to forebody blowing. Furthermore, the solutions obtained in this study are only for the forebody of the aircraft. Thus, the effects of the wing and empennage are not included. Of interest will be the effect of the forebody vortex structure due to the blowing on the vortex breakdown that is known to exist at this angle of attack. Such a breakdown does not occur in the present computations due to the lack of wings in the geometry. In order to determine how the blowing system will work on the full aircraft, experimental and/or computational data using the full aircraft geometry will be required.

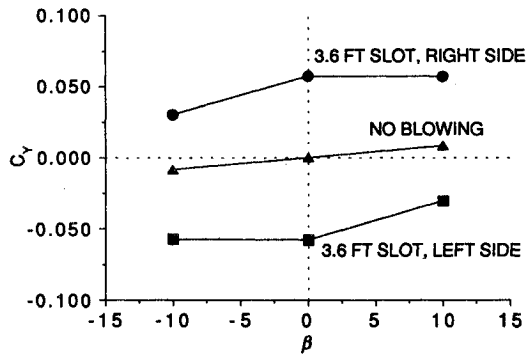

Fig. 13 Effect of sideslip and slot location on the side-force coefficient; $\beta = -10$ deg, $M_\infty = 0.20$, $\alpha = 30$ deg, $Re_c = 11.52 \times 10^6$.

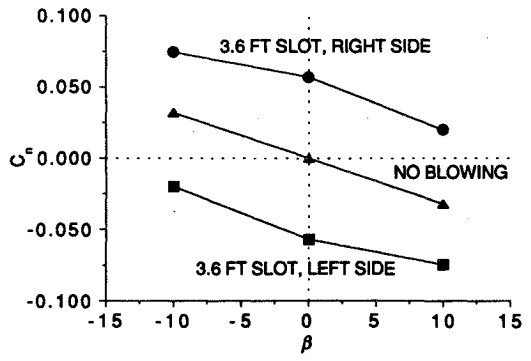

Fig. 14 Effect of sideslip and slot location on the yawing-moment coefficient; $\beta = -10$ deg, $M_\infty = 0.20$, $\alpha = 30$ deg, $Re_c = 11.52 \times 10^6$.

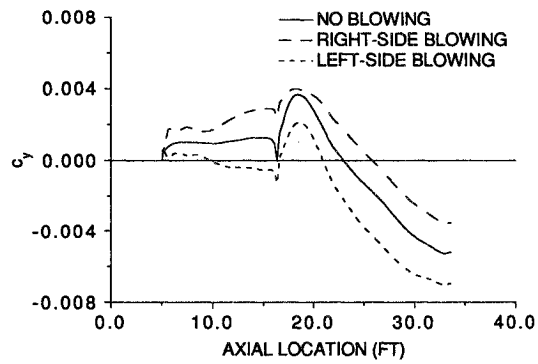

Fig. 15 Effect of sideslip and slot location on side-force distribution; $\beta = -10$ deg, $M_\infty = 0.20$, $\alpha = 30$ deg, $Re_c = 11.52 \times 10^6$.

Conclusions

A computational study of the effectiveness of a tangential forebody slot blowing concept to generate side forces and yawing moments was carried out. The computations were performed on the forebody of the F-18 using a thin-layer Navier-Stokes code. The slot was modeled as an actuator plane. It was found that a short slot placed close to the nose yielded the most side force and yawing moment per unit momentum blowing coefficient. Solutions with a sideslip angle of -10 deg were also obtained. Analysis of these solutions showed that the blowing system generated incremental changes in the side force and yawing moment on order with that obtained from the no-sideslip cases. The results indicate that the interaction of the jet separation vortex with the LEX primary vortices played an important part in the generation of side force and yawing moments.

The computations presented in this study were for the forebody only. The interaction of the flowfield due to blowing with the remainder of the aircraft is not known from these results. Of interest will be the change in the LEX vortex burst point due to blowing and the effect of the altered flowfield on the vertical and horizontal tails. Furthermore, the baseline flow was symmetric, so the effectiveness of the system in asymmetric flows due either to larger angle of attack or asymmetries in the body, need to be investigated. To determine such effects, further computations of the flow about the isolated forebody and the entire aircraft with slot blowing will be necessary. This topic remains a focus of future research.

References

[1]Bowers, A. H., Noffz, G. K., and Peron, L. R., "An Aerodynamic and Jet Deflection Model for Thrust Vectoring on the NASA F/A-18 High-Alpha Research Vehicle," *Proceedings of the NASA High-Angle-of-Attack Technology Conference*, NASA CP 3149, Oct. 1990, pp. 829–862.

[2]Murri, D. G., Biedron, R. T., Erickson, G. E,. Jordan, F. L., and Hoffler, K. D, "Development of Actuated Forebody Strake Controls for the F-18 High-Alpha Research Vehicle," *Proceedings of the NASA High-Angle-of-Attack Technology Conference*, NASA CP 3149, Oct. 1990, pp. 335–380.

[3]Lanser, W. R., and Meyn, L. A., "Forebody Flow Control on a Full-Scale F/A-18 Aircraft," AIAA Paper 92-2674, June 1992.

[4]Ng, T. T., and Malcolm, G. N., "Aerodynamic Control Using Forebody Blowing and Suction," AIAA Paper 91-0619, 1991.

[5]Font, G., and Tavella, D., "High Alpha Aerodynamic Control by Tangential Fuselage Blowing," AIAA Paper 91-0620, Jan. 1991.

[6]Font, G., Celik, Z., and Roberts, L., "A Numerical and Experimental Study of Tangential Jet Blowing Applied to Bodies at High Angles of Attack," AIAA Paper 91-3253, Sept. 1991.

[7]Tavella, D. A., Schiff, L. B., and Cummings, R. M., "Pneumatic Vortical Flow Control at High Angles of Attack," AIAA Paper 90-0098, Jan. 1990.

[8]Murman, S. M., Rizk, Y. M., Cummings, R. M., and Schiff, L. B., "Computational Investigation of Slot Blowing for Fuselage Forebody Flow Control," AIAA Paper 92-0020, Jan. 1992.

[9]Steger, J. L., "Implicit Finite-Difference Simulation of Flow About Arbitrary Two-Dimensional Geometries," *AIAA Journal*, Vol. 16, No. 7, 1978, pp. 679–686.

[10]Steger, J. L., Ying, S. X., and Schiff, L. B., "A Partially Flux-Split Algorithm for Numerical Simulation of Compressible Inviscid and Viscous Flow," *Proceedings of a Workshop on Computational Fluid Dynamics*, Univ. of California, Davis, CA, 1986.

[11]Steger, J. L., and Warming, B. F., "Flux Vector Splitting of the Inviscid Gasdynamics Equations with Applications to Finite-Difference Methods," *Journal of Computational Physics*, Vol. 40, No. 2, 1981, pp. 263–293.

[12]Ying, S. X., Schiff, L. B., and Steger, J. L., "A Numerical Study of Three-Dimensional Separated Flow Past a Hemisphere Cylinder," AIAA Paper 87-1207, June 1987.

[13]Schiff, L. B., Degani, D., and Cummings, R. M., "Computation of Three-Dimensional Turbulent Vortical Flows on Bodies at High Incidence," *Journal of Aircraft*, Vol. 28, No. 11, 1991, pp. 689–699.

[14]Schiff, L. B., Cummings, R. M., Sorenson, R. L., and Rizk, Y. M., "Numerical Simulation of High-Incidence Flow over the F-18 Fuselage Forebody," AIAA Paper 89-0339, Jan. 1989.

[15]Rizk, Y. M., Schiff, L. B., and Gee, K., "Numerical Simulation of the Viscous Flow Around a Simplified F/A-18 at High Angles of Attack," AIAA Paper 90-2999, Aug. 1990.

[16]Rizk, Y. M., and Gee, K., "Numerical Prediction of the Unsteady Flowfield Around the F-18 Aircraft at Large Incidence," AIAA Paper 91-0020, Jan. 1991.

[17]Ying, S. X., "Three-Dimensional Implicit Approximately Factored Schemes for Equations in Gasdynamics," Ph.D. Dissertation, Stanford Univ., Stanford, CA, June, 1986; see also SUDDAR 557, June 1986.

[18]Baldwin, B., and Lomax, H., "Thin-Layer Approximation and Algebraic Model for Separated Turbulent Flows," AIAA Paper 78-0257, Jan. 1978.

[19]Degani, D., and Schiff, L. B., "Computation of Turbulent Supersonic Flows About Pointed Bodies Having Crossflow Separation," *Journal of Computational Physics*, Vol. 66, No. 1, 1986, pp. 173–196.

[20]Roberts, L., "A Theory for Turbulent Curved Wall Jets," AIAA Paper 87-0004, Jan. 1987.

[21]Yeh, D., Tavella, D., and Roberts, L., "Numerical Study of the Effect of Tangential Leading Edge Blowing on Delta Wing Vortical Flow," AIAA Paper 89-0341, Jan. 1989.

[22]Degani, D., and Zilliac, G. G., "Experimental Study of the Nonsteady Asymmetric Flow Around an Ogive-Cylinder at Incidence," *AIAA Journal*, Vol. 28, No. 4, 1990, pp. 642–649.

[23]Degani, D., and Schiff, L. B., "Numerical Simulation of the Effect of Spatial Disturbances on Vortex Asymmetry," *AIAA Journal*, Vol. 29, No. 3, 1991, pp. 344–352.

[24]Degani, D., "Numerical Investigation of the Origin of Vortex Asymmetry," AIAA Paper 90-0593, Jan. 1990.

[25]Levy, Y., Degani, D., and Seginer, A., "Graphical Visualization of Vortical Flows by Means of Helicity," *AIAA Journal*, Vol. 28, No. 8, 1990, pp. 1347–1352.